Modelling Dispersion Compensation in a Cascaded-Fiber-Feedback Optical Parametric Oscillator

optics

MDPI

Article

Modelling Dispersion Compensation in a Cascaded-Fiber-Feedback Optical Parametric Oscillator

Ewan Allan †, Craig Ballantine †, Sebastian C. Robarts, David Bajek and Richard A. McCracken *

Scottish Universities Physics Alliance (SUPA), Institute of Photonics and Quantum Sciences, School of Engineering and Physical Sciences, Heriot-Watt University, Edinburgh EH14 4AS, UK; ea102@hw.ac.uk (E.A.); cb121@hw.ac.uk (C.B.); scr2@hw.ac.uk (S.C.R.); d.bajek@hw.ac.uk (D.B.)

* Correspondence: R.A.McCracken@hw.ac.uk

† These authors contributed equally to this work.

Abstract: Fiber-feedback optical parametric oscillators (OPOs) incorporate intracavity fibers to provide a compact high-energy wavelength-tunable laser platform; however, dispersive effects can limit operation to the sub-picosecond regime. In this research article, we modeled pulse propagation through systems of cascaded fibers, incorporating SMF-28 and ultra-high numerical aperture (UHNA) fibers with complementary second-order dispersion coefficients. We found that the pulse duration upon exiting the fiber system is dominated by uncompensated third-order effects, with UHNA7 presenting the best opportunity to realise a cascaded-fiber-feedback OPO.

Keywords: fiber dispersion; nonlinear optics; optical parametric oscillators

Citation: Allan, E.; Ballantine, C.; Robarts, S.C.; Bajek, D.; McCracken, R.A. Modelling Dispersion Compensation in a Cascaded-Fiber-Feedback Optical Parametric Oscillator. *Optics* **2021**, *2*, 96–102. https://doi.org/10.3390/opt2020010

Academic Editors: Marco Lamperti and Riccardo Gotti

Received: 14 May 2021
Accepted: 27 May 2021
Published: 28 May 2021

Publisher's Note: MDPI stays neutral with regard to jurisdictional claims in published maps and institutional affiliations.

1. Introduction

Optical parametric oscillators (OPOs) provide a versatile platform for the generation of wavelengths ordinarily inaccessible directly from laser gain media [1–3], and have found applications in spectroscopy [4], metrology [5] and multi-photon imaging [6]. Exploiting $\chi^{(2)}$ effects in nonlinear crystals, an OPO acts as a photon splitter, generating longer wavelength signal and idler outputs from a short wavelength pump laser in an energy conserving process. Ultrashort pulsed operation requires synchronous pumping, in which a cavity resonant at the signal wavelength is formed around the nonlinear crystal [7], as illustrated in Figure 1a. A conventional synchronously-pumped OPO has a cavity length L_{OPO} that is inversely proportional to the repetition frequency f_{REP} of its pump laser. The cavity length is selected to provide periodic temporal overlap between the incoming pump and resonant signal pulse trains, with a length directly equal to that of the pump laser providing the highest gain [8]. Meeting these criteria becomes increasingly challenging when moving to a high-energy regime with few-MHz repetition frequencies, as long cavity lengths introduce space and engineering constraints [9].

Fiber-feedback OPOs (Figure 1b) address this issue by placing a single-mode fiber inside the OPO cavity as a length-eating mechanism, exploiting the ∼1.45x optical path reduction in silica-based fibers [10]. Due to the large material dispersion introduced by the fiber, these OPOs have primarily operated in the picosecond regime [11]; however, sub-150-fs femtosecond operation is desirable for many applications but has only been demonstrated in a few instances [12,13]. Intracavity compression using prism or grating pairs is not feasible when longer fiber lengths are employed, and these approaches also introduce additional engineering complexities.

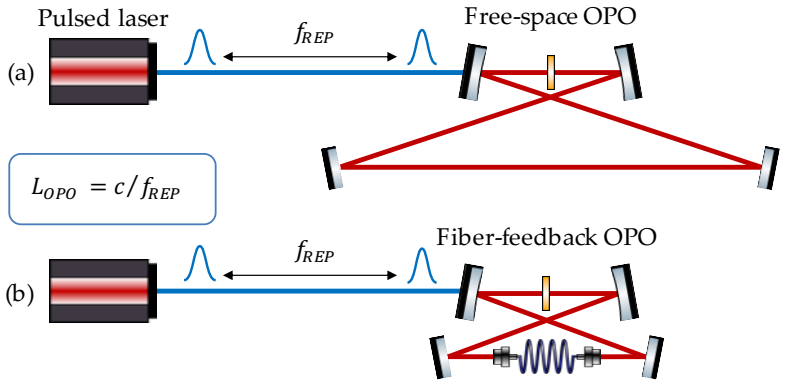

Figure 1. Schematic of a synchronously-pumped OPO. (**a**) A conventional free-space OPO cavity. (**b**) A fiber-feedback OPO using intracavity fiber to reduce the free-space path length.

In this paper, we modeled the net dispersion of cascaded fibers for use in OPOs operating at 1550, 1700 and 2090 nm, wavelengths of interest for infrared material processing [14], three-photon imaging [15] and mid-IR frequency comb applications, respectively [16]. We simulated pulse propagation through lengths of SMF-28 Ultra (Corning) and ultra-high numerical aperture fibers (UHNA, Coherent-Nufern) to identify combinations that balance both second- and third-order dispersive effects to support femtosecond operation.

2. Methods

2.1. Determination of Beta Coefficients

Chromatic dispersion within a fiber can be expressed in terms of phase constant β, which can be expanded as a Taylor series around central frequency ω_0 [17]:

$$\beta(\omega) = \beta_0 + \beta_1(\omega - \omega_0) + \frac{1}{2!}\beta_2(\omega - \omega_0)^2 + \frac{1}{3!}\beta_3(\omega - \omega_0)^3 + \ldots \quad (1)$$

with

$$\beta_m = \frac{d^m}{d\omega^m}\left(n(\omega)\frac{\omega}{c}\right)\Big|_{\omega=\omega_0} \qquad (m = 0, 1, 2\ldots.) \quad (2)$$

where $n(\omega)$ is the refractive index at frequency ω. The second-order dispersion β_2 is responsible for pulse broadening and is given by:

$$\beta_2 = \frac{1}{c}\left(2\frac{dn}{d\omega} + \omega\frac{d^2n}{d\omega^2}\right) \quad (3)$$

However, it is also common to use the alternative representation D to describe the dispersion parameter of a fiber, which is linked to β_2 by:

$$D = -\frac{2\pi c}{\lambda^2}\beta_2 \quad (4)$$

Dispersion information for Coherent-Nufern UHNA fibers was not available from the manufacturer; however, measurements of dispersion parameter D were carried out by Ciąćka et al. [18] over the 1400–2200 nm wavelength region using spectral interferometry [19,20]. Their results also provided good agreement with dispersion measurements of Corning SMF-28 Ultra over the 1200–1625 nm range specified by the manufacturer [21]. We extracted numerical data for D for SMF-28 Ultra, UHNA1, UHNA3, UHNA4 and UHNA7 from [18] using the free software WebPlotDigitzer [22], with around 40 points collected per data set across each wavelength range. Fitting to this data and evaluating at a higher point density provided increased resolution (Figure 2a). The second-order dispersion β_2 was calculated from Equation (4), and a multi-order polynomial fit applied to evaluate the dispersion coefficients from β_2 to β_n, evaluated at $\omega - \omega_0$, where ω_0 is a

frequency corresponding to a selected wavelength of interest (Figure 2b). The calculated β_2 and β_3 coefficients for each fiber, evaluated at 1550, 1700 and 2090 nm, are shown in Table 1 and Table 2, respectively. Uncertainties in our approach are dominated by the standard deviations reported in [18]; however, these only introduce a <1% error in our calculations of β_2 and β_3.

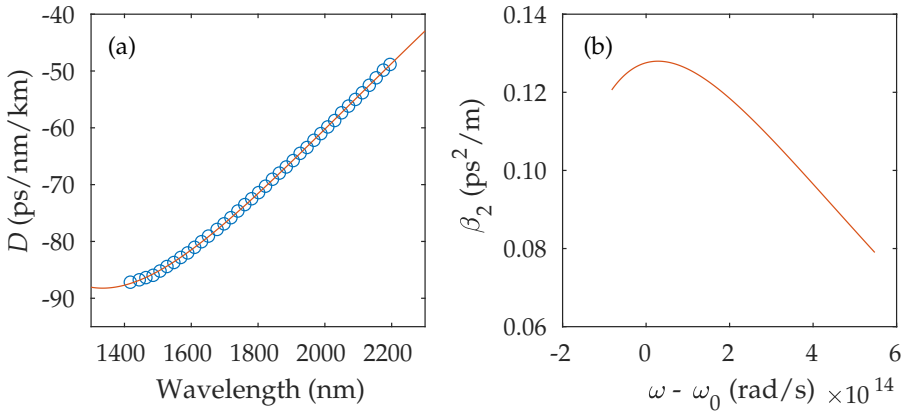

Figure 2. (**a**) UHNA3 dispersion parameter D, with data points extracted from Figure 4 of [18] (blue circles) and fitted curve (red line). (**b**) UHNA3 β_2 coefficient evaluated at $\omega_0 \mathrel{\widehat{=}} 2090$ nm.

Table 1. β_2 coefficients (ps^2/m).

	SMF-28	**UHNA1**	**UHNA3**	**UHNA4**	**UHNA7**
1550 nm	−0.0215	0.0436	0.1065	0.0694	0.0263
1700 nm	−0.0371	0.0463	0.1178	0.0814	0.0316
2090 nm	−0.0852	0.0207	0.1276	0.0801	0.0514

Table 2. β_3 coefficients (ps^3/km).

	SMF-28	**UHNA1**	**UHNA3**	**UHNA4**	**UHNA7**
1550 nm	0.1256	−0.0392	−0.1133	−0.1149	−0.0402
1700 nm	0.1679	−0.0023	−0.0947	−0.1006	−0.0603
2090 nm	0.3173	0.3384	0.0290	0.2062	−0.1452

2.2. Pulse Propagation Model

To model pulse propagation in different fibers, we simulated a temporal electric field with a Gaussian pulse envelope of the following form:

$$E(t) \propto \exp\left(-\frac{[2\ln 2]t^2}{\Delta\tau^2}\right) \tag{5}$$

where $\Delta\tau$ is the full-width half-maximum (FWHM) of the temporal intensity. The spectral field can be obtained via Fourier transform of the temporal field:

$$E(\omega) = \int_{-\infty}^{+\infty} E(t)e^{-i\omega t}\,dt \tag{6}$$

The spectral phase accumulated by propagation through fiber length L with phase constant β was added to $E(\omega)$, with the resultant change in pulse duration obtained by inverse Fourier transform:

$$E(t,L) = \frac{1}{\sqrt{2\pi}}\int_{-\infty}^{+\infty} E(\omega)e^{-i\beta L}e^{i\omega t}\,d\omega \tag{7}$$

We selected an input pulse duration of $\Delta\tau$ = 50 fs and a length resolution of dL = 5 mm. The UHNA fibers have core diameters $\leq$ 2.5 µm [23], presenting an acute coupling challenge. We addressed this by using SMF-28 Ultra as an input/output coupler, taking advantage of the larger 8.2 µm core diameter and connectorized end facets, resulting in a cascaded SMF-28/UHNA/SMF-28 fiber system. Losses between these mismatched cores can be as low as ~0.3 dB when using a "fire polish" thermal diffusion splice [13]. Component fiber lengths were selected such that the net second-order dispersion after 1 m of propagation was close to zero, within the 5 mm resolution of our simulation. SMF-28 possesses negative β_2 at our test wavelengths, while all UHNA fibers have positive β_2 coefficients, providing compensation of second-order dispersive effects. Individual fiber lengths are shown in Table 3, and were determined by the absolute ratio of the β_2 coefficients in the cascaded SMF-28/UHNA/SMF-28 system, such that:

$$\frac{L_{\text{SMF-28}}}{L_{\text{UHNA}}} = \left| \frac{\beta_{2(\text{UHNA})}}{2\,\beta_{2(\text{SMF-28})}} \right| \tag{8}$$

Table 3. Length ratios minimising β_2 through 1-m of cascaded SMF-28/UHNA/SMF-28 fibers.

	UHNA1	**UHNA3**	**UHNA4**	**UHNA7**
1550 nm	0.325/0.35/0.325	0.41/0.18/0.41	0.38/0.24/0.38	0.275/0.45/0.275
1700 nm	0.265/0.47/0.265	0.38/0.24/0.38	0.34/0.32/0.34	0.23/0.54/0.23
2090 nm	0.09/0.82/0.09	0.30/0.40/0.30	0.235/0.53/0.235	0.185/0.63/0.185

3. Results and Discussion

In Figures 3–6, we plotted the results of our fiber dispersion model, along with output pulse profiles after propagation through the cascaded system. Stepwise animations of pulse propagation through each fiber combination at a wavelength of 2090 nm are available as Supplementary Files.

The normalized FWHM output duration was calculated at each wavelength for comparison against the 50 fs input pulse. With fiber lengths selected to minimize second-order dispersion, pulse broadening is dominated by uncompensated third-order contributions. SMF-28 possesses positive β_3 that increases with wavelength; therefore, the UHNA fibers must provide negative β_3 contributions to prevent pulse breakup.

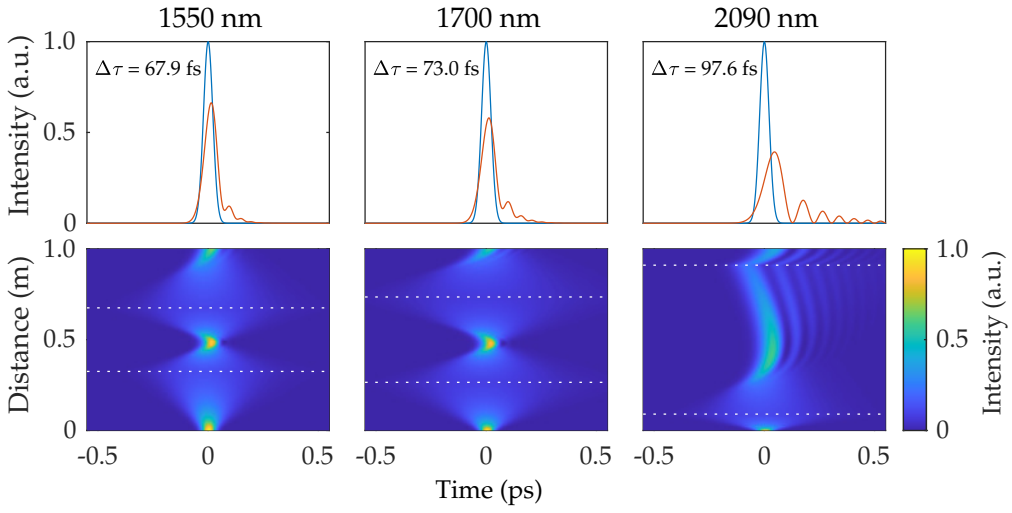

Figure 3. Top row: pulse temporal intensity before (blue) and after (red) propagation through SMF-28 and UHNA1. Bottom row: evolution of the temporal intensity profile through the system of cascaded fibers. White lines indicate transitions between different fibers.

The cascaded UHNA1 system (Figure 3) displayed moderate broadening at 1550 and 1700 nm, with net positive third-order dispersion producing a trailing pulse edge. Oscillations in the pulse envelope did not drop to zero; therefore, the pulse remained intact. However, at 2090 nm, both SMF-28 and UHNA1 had large β_3 coefficients (>0.31 ps^3/km) and the pulse broke up, with only 76% of the input energy remaining in the primary pulse.

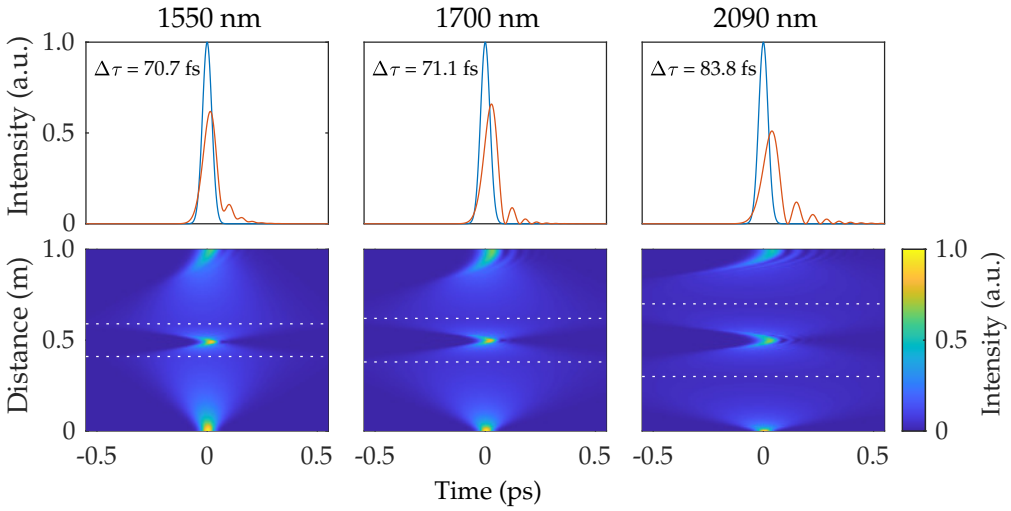

Figure 4. Top row: pulse temporal intensity before (blue) and after (red) propagation through SMF-28 and UHNA3. Bottom row: evolution of the temporal intensity profile through the system of cascaded fibers. White lines indicate transitions between different fibers.

UHNA3 displayed high β_2 values (>0.1 ps^2/m) and, therefore, longer lengths of SMF-28 are required in this cascaded system (Figure 4). Uncompensated third-order terms were positive at all test wavelengths, and pulse breakup was evident at 2090 nm.

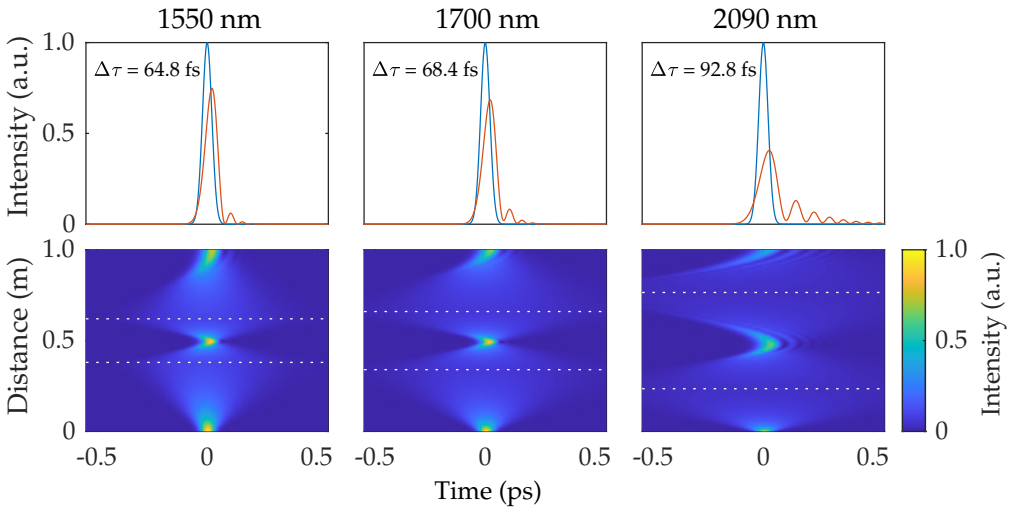

Figure 5. Top row: pulse temporal intensity before (blue) and after (red) propagation through SMF-28 and UHNA4. Bottom row: evolution of the temporal intensity profile through the system of cascaded fibers. White lines indicate transitions between different fibers.

Results for UHNA4 are shown in Figure 5. Both UHNA3 and UHNA4 possessed similar β_3 coefficients at 1550 and 1700 nm, and both fibers displayed similar amounts of broadening. At 2090 nm, UHNA4 had a large positive β_3 which, when combined with the SMF-28, created significant pulse breakup, again with around 75% of the energy remaining in the primary pulse.

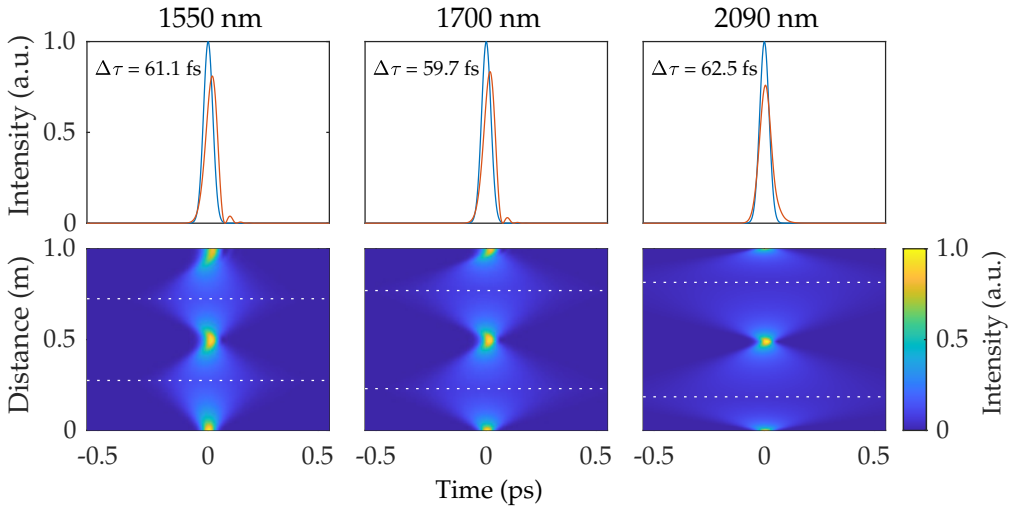

Figure 6. Top row: pulse temporal intensity before (blue) and after (red) propagation through SMF-28 and UHNA7. Bottom row: evolution of the temporal intensity profile through the system of cascaded fibers. White lines indicate transitions between different fibers.

UHNA7 differed from the other fibers in that it had a low and flat β_2 curve, but also displayed negative β_3 at all test wavelengths. With both second- and third-order coefficients opposite in sign to those of SMF-28, it presents the best opportunity for dispersion compensation in a fiber-feedback OPO. The pulse propagation results for UHNA7 are shown in Figure 6. At all wavelengths, pulse broadening was minimal, with the shortest pulses observed in our model (59.7 fs) found when using UHNA7 at 1700 nm. This agrees with the experimental results reported in [13], which incorporated cascaded SMF-28/UHNA7/SMF-28 in a degenerate OPO operating at 2090 nm.

4. Conclusions

We modeled pulse propagation through systems of cascaded SMF-28 and UHNA fibers for use in fiber-feedback optical parametric oscillators. Dispersion curves were extracted from [18] using freely available software [22] and evaluated at key wavelengths of interest to the ultra-fast community. We observed that uncompensated third-order dispersion dominates in a cascaded fiber system, and will produce pulse breakup in many UHNA fibers at 2090 nm. The design of UHNA7 produced negative β_3 coefficients that complemented the positive third-order dispersion of SMF-28, leading to minimal pulse broadening after propagation along 1 m of cascaded fiber. Our results will serve as a guideline for the design of fiber-feedback OPOs operating in the few-MHz regime and incorporating longer lengths of fiber.

Supplementary Materials: The following are available online at https://www.mdpi.com/article/10.3390/opt2020010/s1, Video S1: Pulse propagation through cascaded SMF-28/UHNA1/SMF-28 fibers at 2090 nm, Video S2: Pulse propagation through cascaded SMF-28/UHNA3/SMF-28 fibers at 2090 nm, Video S3: Pulse propagation through cascaded SMF-28/UHNA4/SMF-28 fibers at 2090 nm, Video S4: Pulse propagation through cascaded SMF-28/UHNA7/SMF-28 fibers at 2090 nm.

Author Contributions: Conceptualization, supervision, project administration, funding acquisition and writing—original draft preparation, R.A.M.; software, investigation and methodology, C.B. and S.C.R.; validation, visualization and writing—review and editing, E.A. and D.B. All authors have read and agreed to the published version of the manuscript.

Funding: This research was funded by the Science and Technologies Facilities Council, grant number ST/T000651/1.

Conflicts of Interest: The authors declare no conflicts of interest.

References

1. Ghotbi, M.; Esteban-Martin, A.; Ebrahim-Zadeh, M. BiB_3O_6 femtosecond optical parametric oscillator. *Opt. Lett.* **2006**, *31*, 3128–3130. doi:10.1364/OL.31.003128.
2. Gu, C.; Hu, M.; Fan, J.; Song, Y.; Liu, B.; Chai, L.; Wang, C.; Reid, D.T. High power tunable femtosecond ultraviolet laser source based on an Yb-fiber-laser pumped optical parametric oscillator. *Opt. Express* **2015**, *23*, 6181–6186. doi:10.1364/OE.23.006181.
3. Maidment, L.; Schunemann, P.G.; Reid, D.T. Molecular fingerprint-region spectroscopy from 5 to 12 μm using an orientation-patterned gallium phosphide optical parametric oscillator. *Opt. Lett.* **2016**, *41*, 4261–4264. doi:10.1364/OL.41.004261.
4. Johnson, K.; Castro-Marin, P.; Kara, O.; Farrell, C.; Reid, D.T. High resolution ZrF_4-fiber-delivered multi-species infrared spectroscopy. *OSA Contin.* **2020**, *3*, 3595–3603. doi:10.1364/OSAC.412207.
5. Balskus, K.; Schilt, S.; Wittwer, V.J.; Brochard, P.; Ploetzing, T.; Jornod, N.; McCracken, R.A.; Zhang, Z.; Bartels, A.; Reid, D.T.; et al. Frequency comb metrology with an optical parametric oscillator. *Opt. Express* **2016**, *24*, 8370–8381. doi:10.1364/OE.24.008370.
6. Kobat, D.; Horton, N.G.; Xu, C. In vivo two-photon microscopy to 1.6-mm depth in mouse cortex. *J. Biomed. Opt.* **2011**, *16*, 1–5. doi:10.1117/1.3646209.
7. Edelstein, D.C.; Wachman, E.S.; Tang, C.L. Broadly tunable high repetition rate femtosecond optical parametric oscillator. *Appl. Phys. Lett.* **1989**, *54*, 1728–1730. doi:10.1063/1.101272.
8. Kimmelma, O.; Kumar, S.C.; Esteban-Martin, A.; Ebrahim-Zadeh, M. Multi-gigahertz picosecond optical parametric oscillator pumped by 80-MHz Yb-fiber laser. *Opt. Lett.* **2013**, *38*, 4550–4553. doi:10.1364/OL.38.004550.
9. Lamour, T.P.; Reid, D.T. 650-nJ pulses from a cavity-dumped Yb:fiber-pumped ultrafast optical parametric oscillator. *Opt. Express* **2011**, *19*, 17557–17562. doi:10.1364/OE.19.017557.
10. Südmeyer, T.; der Au, J.A.; Paschotta, R.; Keller, U.; Smith, P.G.R.; Ross, G.W.; Hanna, D.C. Femtosecond fiber-feedback optical parametric oscillator. *Opt. Lett.* **2001**, *26*, 304–306. doi:10.1364/OL.26.000304.
11. Kienle, F.; Teh, P.S.; Alam, S.U.; Gawith, C.B.E.; Hanna, D.C.; Richardson, D.J.; Shepherd, D.P. Compact, high-pulse-energy, picosecond optical parametric oscillator. *Opt. Lett.* **2010**, *35*, 3580–3582. doi:10.1364/OL.35.003580.
12. O'Donnell, C.F.; Kumar, S.C.; Paoletta, T.; Ebrahim-Zadeh, M. Widely tunable femtosecond soliton generation in a fiber-feedback optical parametric oscillator. *Optica* **2020**, *7*, 426–433. doi:10.1364/OPTICA.391025.
13. Ingold, K.A.; Marandi, A.; Digonnet, M.J.F.; Byer, R.L. Fiber-feedback optical parametric oscillator for half-harmonic generation of sub-100-fs frequency combs around 2 μm. *Opt. Lett.* **2015**, *40*, 4368–4371. doi:10.1364/OL.40.004368.
14. Nejadmalayeri, A.H.; Herman, P.R.; Burghoff, J.; Will, M.; Nolte, S.; Tünnermann, A. Inscription of optical waveguides in crystalline silicon by mid-infrared femtosecond laser pulses. *Opt. Lett.* **2005**, *30*, 964–966. doi:10.1364/OL.30.000964.
15. Ouzounov, D.; Wang, T.; Wang, M.; Feng, D.D.; Horton, N.G.; Cruz-Hernández, J.C.; Cheng, Y.T.; Reimer, J.; Tolias, A.S.; Nishimura, N.; et al. In vivo three-photon imaging of activity of GCaMP6-labeled neurons deep in intact mouse brain. *Nat. Methods* **2017**, *14*, 388–390. doi:10.1038/nmeth.4183.
16. Schliesser, A.; Picqué, N.; Hänsch, T.W. Mid-infrared frequency combs. *Nat. Photon.* **2012**, *6*, 440–449. doi:10.1038/nphoton.2012.142.
17. Agrawal, G.P. *Nonlinear Fiber Optics*; Academic Press: Cambridge, MA, USA, 2001; pp. 1–30; Volume 3.
18. Ciąćka, P.; Rampur, A.; Heidt, A.; Feurer, T.; Klimczak, M. Dispersion measurement of ultra-high numerical aperture fibers covering thulium, holmium, and erbium emission wavelengths. *J. Opt. Soc. Am. B* **2018**, *35*, 1301–1307. doi:10.1364/JOSAB.35.001301.
19. Merritt, P.; Tatam, R.; Jackson, D. Interferometric chromatic dispersion measurements on short lengths of monomode optical fiber. *J. Light. Technol.* **1989**, *7*, 703–716. doi:10.1109/50.19099.
20. Hlubina, P.; Kadulová, M.; Ciprian, D. Spectral interferometry-based chromatic dispersion measurement of fibre including the zero-dispersion wavelength. *J. Eur. Opt. Soc. Rapid Publ.* **2012**, *7*. doi:10.2971/jeos.2012.12017.
21. Corning SMF-28 Ultra Optical Fiber Product Information. Available online: https://www.corning.com/media/worldwide/coc/documents/Fiber/SMF-28%20Ultra.pdf (accessed on 22 April 2021).
22. Rohatgi, A. Webplotdigitizer: Version 4.4. Available online: https://automeris.io/WebPlotDigitizer (accessed on 22 April 2021).
23. Coherent-Nufern UHNA Fiber Product Information. Available online: https://www.nufern.com/pam/optical_fibers/spec/id/988/?2141 (accessed on 22 April 2021).